IET Control Theory & Applications

Special Section: Emerging Trends in LPV-Based Control of Intelligent Automotive Systems

IET Journals
The Institution of Engineering and Technology

Reference-free approach for mitigating human–machine conflicts in shared control of automated vehicles

ISSN 1751-8644
Received on 6th March 2020
Revised 22nd April 2020
Accepted on 9th June 2020
E-First on 8th October 2020
doi: 10.1049/iet-cta.2020.0289
www.ietdl.org

Chao Huang[1], Chen Lv[1] ✉, Fazel Naghdy[2], Haiping Du[2]

[1]*School of mechanical and Aerospace Engineering, Nanyang Technological University, Singapore, 639798, Singapore*
[2]*Faculty of Engineering and Information Sciences, School of Electrical, Computer and Telecommunications Engineering, University of Wollongong, Wollongong, 2500, NSW, Australia*
✉ *E-mail: lyuchen@ntu.edu.sg*

Abstract: Shared control is a promising approach that can facilitate the mutual understanding and cooperative control between human and machine. In this study, a novel reference-free framework for shared control of automated vehicles is proposed with the aim of mitigating conflicts between the human driver and the automatic system during their interactions. Position constraint and time to collision are deployed to prevent collision and guarantee stability by limiting the yaw rate and sideslip angle of the vehicle. The design of the shared controller is formulated as a model predictive control problem. It determines vehicle state based on the current driver command and implements control actions only if the vehicle state induced by the human driver violates the pre-defined constraints. The system models, safety constraints and the proposed shared controller are then integrated. The algorithm is validated through computer simulation under two different driving scenarios. The simulation results show that the proposed reference-free approach can offer the human driver more degrees of freedom during shared control, effectively mitigating human–machine conflicts, compared to the previous work. In addition, the algorithm ensures the safety and stability of the system under risky driving conditions, validating its feasibility and effectiveness.

Nomenclature

$\mathbf{0}$	zero matrix with appropriate dimension
$\mathbf{R}^{n\times m}$	$n \times m$ matrix
α_f, α_r	slip angle for the front wheel and rear wheel
β	sideslip angle
δ_a	automation's steering angle
δ_d	driver's steering angle
ψ	inertial heading angle
F_{cf}, F_{cr}	lateral tyre forces at the front and rear wheels, respectively
H_c	control horizon
H_p	prediction horizon
r	Yaw rate
T_a	automation's acceleration/brake torque
T_d	driver's acceleration/brake torque
T_p	sampling time
T_r	real wheel traction or brake torque
v_x, v_y	longitudinal and lateral speeds of the centre of mass of vehicle
X, Y	position of the vehicle in global word coordinate
$C_{\alpha_f}, C_{\alpha_r}$	cornering stiffness of the front tyre, rear tyre
I_z	vehicle's yaw inertia
l_f, l_r	distance from the centre of gravity to the front and rear wheel
m	vehicle's mass
R_w	rolling radius

1 Introduction

Autonomous vehicles are expected to handle a larger amount of information and process them faster in order to achieve a lower rate of traffic accidents than those caused by human errors [1–4]. However, the autonomous vehicles cannot be produced and deployed on a wide scale until some important issues, such as public acceptance and liability issues, are addressed [5]. The literature on human factors in vehicle automation pointed out that the autonomous driving technology is not fully capable of making human-like decisions and judgment calls so far. In addition, this technology is sensitive to complex driving situations, such as bad weather conditions [6]. Lu *et al.* [7] found that a high level of automation can render human driver skill degradation, increase mental overload and cause the loss of situation awareness. Many scholars remain sceptical of the technology behind autonomous and state that the automated vehicle may not be fully adopted by the majority of the population in the foreseeable future until further testing could be completed [8].

To bridge the gaps mentioned above, the shared control approach between human driver and automated vehicle may be promising as an alternative driving mode and considered as an intermediate step towards full autonomous driving [9]. As we know, the human drivers can access to a rich set of sensory information offering superior perception and judgment, and drive the vehicle in complex driving scenarios while automation excels at precisely executing actions over lateral and longitudinal positioning. Thus, a shared control system can combine the driver's and automation's benefits [10]. Shared control approaches have been successfully applied in many fields, including automobile [11], aircraft [12] and surgery [13]. An example of shared control in automotive applications is the lane keeping assistant system, where the human driver and automation contribute simultaneously to the steering wheel to control the vehicle within the lane [14].

The main communication between vehicle and human during their collaboration is through a human–machine interface (HMI). Based on the types of HMI, the shared control system can be divided into multiple modalities, including visual, auditory, haptic and mixture types. Rather than representing the continuously support to the human driver, visual and auditory interfaces are more like warning functionalities to alarm the human driver when risk level increases [15]. However, the visual display may require the driver frequently reallocate their attentions from the road to the display interface and the auditory display may easily lead to irritations on humans. In this context, haptic shared control (HSC) becomes more promising as it enables the human driver to communicate continuously with automation through a haptic interface [16]. By using the haptic interface, such as joystick or steering wheel, the driver can feel the additional force or torque,

sensing the information conveyed by the automation, and then make a decision on future actions [17]. The multi-modal HSC is shown to capture the driver's attention more effectively and provide a more natural interaction [18, 19]. Multiple studies show that the HSC improved driving performance in both lateral (via a haptic steering wheel) direction and longitudinal direction (via a haptic pedal) [20, 21]. For the haptic pedal shared control system, it supports drivers to control the longitudinal motion of vehicle, addressing speed adaption and collision avoidance. For example, in the car following system, a haptic feedback force, which is generated and worked on the gas pedal, is complemented to maintain a constant distance between the vehicle and the front vehicle [22–24]. The study of haptic steering control system attracts more concerns since the research has shown that human drivers tend to steer first before using the pedals when confronted with system failures [25]. Comprehensive studies have been explored in existing studies [17, 20, 26–28].

According to the level of autonomy, the shared control systems can be classified into two types: the lower automation mode and higher automation one. In the lower automation mode, the human driver is responsible for monitoring the driving environment and is expected to be available for control at all times. While in the higher automation mode, the human driver is the main fallback and only responsible for higher level control operations such as decision making [29].

Based on the different control logic, the shared control algorithms can be divided into two categories: the path-based approach and the reference-free one. In the path-based approach, the path planning methods, including model predictive control (MPC) [30], rapidly exploring random trees [31] and geometric method [32], are utilised to identify an optimal path among all available and feasible trajectory options. The automation continuously supports the driver to follow the optimal path, keeping the driver in the control loop [33–35]. This approach can ensure the controllability and the feasibility of vehicle motion and reduce the driver's control effort, especially in emergency situations [16]. However, it would inevitably lead to conflicts between the driver and the automation when both of them control the vehicle simultaneously. Therefore, how to dynamically allocate the control authority and improve the mutual understanding between the human driver and automation in the execution of the driving task are challenging and worthwhile exploring [36]. Another drawback of the path-based approach is it heavily relies on the so-called optimal path which is defined and generated by the automation itself. More specifically, the determination of the optimal path should not only depend on safety and efficiency, but also need to be associated to human drivers' characterisations (e.g. driving styles, skills, habits, preferences etc.). A non-adaptive optimal path may over-restrict driver's driving freedom, and a continuous assistance force may be considered annoying when the driver deems the situation safe [37]. In a reference-free approach, the driver can dominate the control by presenting his or her command (e.g. lane change intention), while the automation works as a supervisor to monitor the human driver's states (e.g. drowsiness and gaze) and environment, following the driver's command. The automation system will be responsible for taking appropriate corrective actions if necessary. Even though the automation can generate possible decision options, the vehicle's actual guidance is carried out by the human driver, and the automation only offers additional control effort when the vehicle state is about to exceed the predefined safety threshold [38, 39]. The biggest benefit it offers is that the driver retains as much direct control freedom as possible [40]. The drivers can feel the responses of their control actions immediately, and therefore further execute appropriate control actions based on their understanding of the current situation.

In this paper, we propose a novel reference-free framework for the shared control system of automated vehicles, with the aim of mitigating conflicts between human driver and the automation functionality during their interactions. We utilise the safety constraints for collision avoidance and stability guarantee in the driving task. In particular, constrained Delaunay triangles and time to collision (TTC) are utilised to identify the collision-free area. In addition, the boundaries on the sideslip angle and yaw rate of the vehicle are considered and applied to guarantee the vehicle's stability and handling performance. In normal situations, the human drivers make decisions based on their own evaluation of the situation, and the driver's inputs, such as steering wheel angle and pedal force, which are imported to the electric control unit of vehicle to execute the appropriate actions. Once the vehicle is potential against the safety constraints and an unsafe situation is announced, interventions including steering wheel angle and acceleration/braking torque are generated by a predictive controller to correct vehicle's lateral and longitudinal behaviours. In the developed shared control algorithm, the predicted driver behaviour, vehicle's states and safety constraints are formulated to determine the minimum intervention actions in order to keep the vehicle in a safe region. The contributions of this paper can be summarised as follows: (i) a novel reference-free shared control framework is proposed to mitigate human–machine conflicts; (ii) collision-free channels are constructed for automated vehicles by using constrained Delaunay triangulation; (iii) a multi-objective optimisation problem is formulated for human–machine collaborative interactions, ensuring the driver's individual preference, the safety and stability of the system simultaneously.

The remainder of the paper is structured as follows. The high-level system structure is described in Section 2. In Section 3, the vehicle dynamics model is developed for controller design, and the safety constraints are described in details. The proposed reference-free shared control approach is formulated as a prediction optimisation problem in Section 4. The simulation results are demonstrated in Section 5. Section 6 concludes this paper.

2 High-level framework of the shared control system

In this paper, we develop a novel reference-free shared control system for automated vehicles. As shown in Fig. 1, the high-level framework includes human control inputs, the vehicle automation system and the proposed shared control interface. Based on the perception and judgment of the surrounding environment, the human driver makes a high-level decision, such as lane-change, or car-following, and then executes the driving tasks by steering the hand wheel and/or pressing the pedals.

For the vehicle automation system, it is equipped with multi-source sensors, which can measure vehicle states (e.g. velocity, acceleration, yaw movement etc.) and environmental information (e.g. obstacle's position and speed) in real time. What is more, the HMI module works as a communication channel, so that the driver's command can be converted to a steering angle and acceleration/brake torque. In the meantime, additional assistant or correctional information would also be delivered by the automation to the human driver via this HMI.

The shared control system, which is based on the vehicle states and environmental information, modifies the driver's inputs and generates corrected actions through a MPC controller if necessary. The design of the proposed shared control system is described in the following sections.

3 Control-oriented vehicle models and safety constraints

In the proposed shared control approach, the vehicle model is utilised to predict the vehicle's states so that the MPC controller can detect and identify the potential risks like collisions or oversteer. Safety constraints are introduced in Section 3.2.

3.1 Vehicle model

The dynamics of the vehicle is modelled by the following set of differential equations (Fig. 2):

$$
\begin{aligned}
\dot{v}_x &= rv_y - \frac{2}{m}(F_{\mathrm{cf}}\sin\delta_{\mathrm{f}} - T_{\mathrm{r}}/R_w),\\
\dot{v}_y &= -rv_x + \frac{2}{m}(F_{\mathrm{cf}}\cos\delta_{\mathrm{f}} + F_{\mathrm{cr}}),\\
\dot{r} &= \frac{2}{I_z}(l_{\mathrm{f}}F_{\mathrm{cf}} - l_{\mathrm{r}}F_{\mathrm{cr}}),\\
\dot{X} &= v_x\cos\psi - v_y\sin\psi,\\
\dot{Y} &= v_x\sin\psi + v_y\cos\psi\,.
\end{aligned}
\tag{1}
$$

where x and y are the coordinates of the centre of mass (CM) in an inertial frame (X,Y). v_x and v_y are the longitudinal and lateral speeds, respectively. ψ is the inertial heading angle and r is the yaw rate. m and I_z denote the vehicle's mass and yaw inertia, respectively. l_{f} and l_{r} represent the distance from CM to the front and rear axles, respectively. $\dot{X}$ and $\dot{Y}$ denote the longitudinal and lateral speeds of CM in the body frame (X,Y), respectively. The systems' input signals are front wheel angle δ_{f} and real wheel traction or brake torque T_{r}.

We make use of the following assumption on the steering angle.

Assumption 1: It is assumed only the front wheels can be controlled and the steering angle of both front right wheel and front left wheel are the same, i.e. $\delta_{fr} = \delta_{fl} = \delta_{\mathrm{f}}$. In addition, the front wheel angle consists of two parts: $\delta_{\mathrm{f}} = \delta_{\mathrm{d}} + \delta_{\mathrm{a}}$, in which, δ_{d} is the driver-commanded steering angle while δ_{a} is the corrected steering angle provided by the automation. Similarly, $T_{\mathrm{r}} = T_{\mathrm{a}} + T_{\mathrm{d}}$ in which T_{d} is the acceleration/brake torque given by the human driver and T_{a} is the corrected torque provided by the automation.

F_{cf} and F_{cr} denote the lateral tyre forces at the front and rear wheels, respectively. $F_{ci}, (i = f, r)$ can be calculated using a modified non-linear Fiala tyre model [41]

$$
F_{ci} = \begin{cases} -C_{\alpha_i}\tan\alpha_i + \dfrac{C_{\alpha_i}^2}{3\mu F_{z_i}}\tan\alpha_i \left|\tan\alpha_i\right| - \dfrac{C_{\alpha_i}^3}{27(\mu F_{z_i})^2}\tan\alpha_i^3, & \\ \qquad\qquad |\alpha_i| < \alpha_{sl}, \\ -\mu F_{z_i}\mathrm{sgn}(\alpha_i), \qquad |\alpha_i| \le \alpha_{sl}\,. \end{cases}
\tag{2}
$$

where $\alpha_{sl} = \tan^{-1}(3\mu F_z/C_\alpha)$. $\alpha_i, (i = f, r)$ denotes tyre slip angle, which can be expressed as

$$
\begin{aligned}
\alpha_{\mathrm{f}} &\simeq \frac{v_y + l_{\mathrm{f}}r}{v_x} - \delta_{\mathrm{f}}\\
\alpha_{\mathrm{r}} &\simeq \frac{v_y - l_{\mathrm{r}}r}{v_x}\,.
\end{aligned}
\tag{3}
$$

Combining (1)–(3) and considering the driver's inputs are given, we can have the following compact form of vehicle dynamics:

$$
\dot{x}(t) = f(x(t), u(t))\,. \tag{4}
$$

where $x = [X,\ Y,\ r,\ v_x,\ v_y,\ \psi]^{\mathrm{T}}$ and $u = [\delta_{\mathrm{a}}\ T_{\mathrm{a}}]^{\mathrm{T}}$ are the system state vector and input vector, respectively.

3.2 Safety constraints

We consider three aspects of safety constraints: environmental safety, performance safety and operation safety. In the view of environmental safety, it is guaranteed to have no potential rear-on or lateral collisions by introducing position constraint and TTC. During the vehicle operation, the loss in yaw stability may result in oversteer or understeer which can cause the steering become useless, the vehicle spin and all directional control get lost. Therefore, we constrain the sideslip angle and yaw rate, which are the two factors related to the yaw stability, to guarantee the driving performance safety [42]. In addition, we limit the input variables of the vehicle to ensure the stable operation of the automated vehicle. The constraints mentioned above will be discussed below and implemented in the predictive optimisation problem in Section 4.

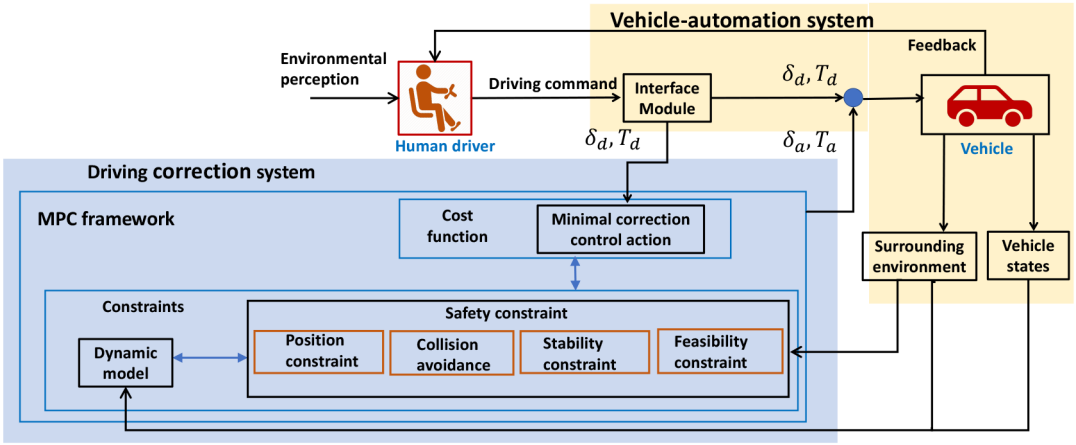

Fig. 1 *Structure of the proposed shared control system*

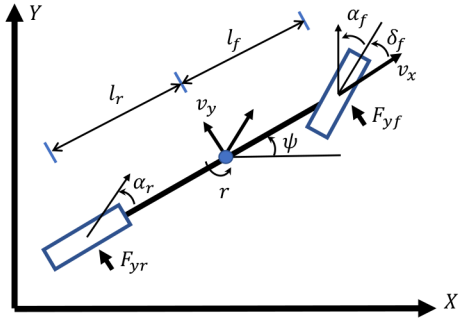

Fig. 2 *Vehicle model*

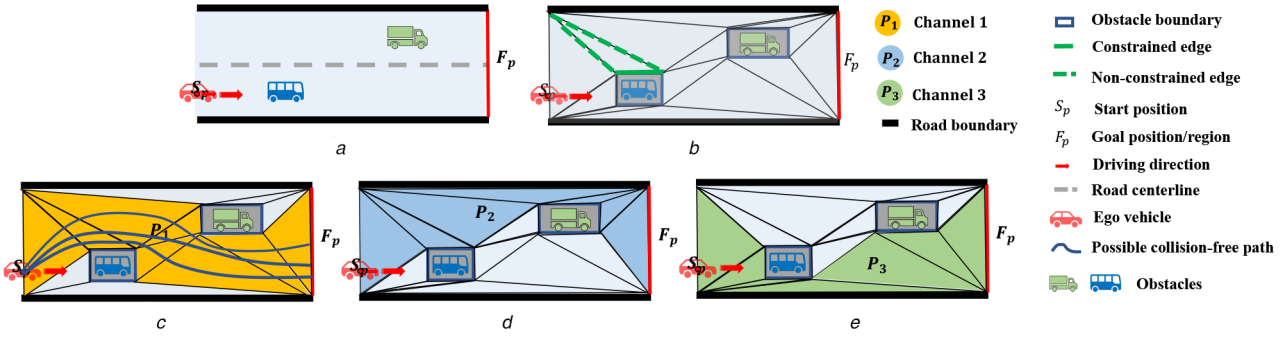

Fig. 3 *Illustration of collision-free channels based on constrained Delaunay triangulation*
(a) Driving region, ***(b)*** Discretised region with CDT, ***(c)*** Channel 1, ***(d)*** Channel 2, ***(e)*** Channel 3

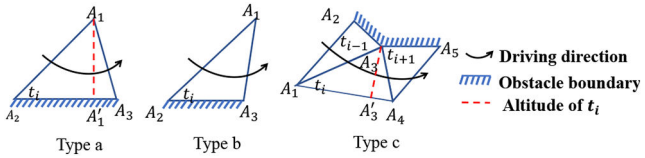

Fig. 4 *Width of triangle t_i*

3.2.1 Position constraints: Constrained Delaunay triangulation can partition driving environment into a set of triangles where the vehicle can travel from triangle to triangle without potential collisions and has been widely used in path planning [43] and pathfinding problem [44]. Compared with other cellular methods, it requires less data storage about environment information and is more helpful to plan further reasonable motion [45]. Given a driving region (Fig. 3*a*), the obstacles and boundaries are described by line segments. The environment can be discretised into several triangles by inserting edges between these line segments' endpoints. It should be noticed that the obstacle's barriers are required to be the (constrained) edges in the triangulation so that the possible path we find cannot cross the barriers of the obstacles (Fig. 3*b*). Rather than finding a shortest point-to-point path in the driving region, we prefer to identify a set of safe area for the vehicle to stay inside. The following assumption is given.

Assumption 2: In the driving region, the environmental information such as lane numbers, obstacle velocity and positions are assumed known by the current sensor technologies over a finite preview horizon. The above information can be obtained at each time step and the corresponding constrained Delaunay triangulation graph can be dynamically updated by considering the changes in the environment.

Based on the known environmental information, the driving region can be discretised into constrained Delaunay triangles. Each sequence of adjacent Delaunay triangles connecting the start position S_p with a goal point/goal region F_p can constitute a channel.

Definition 1: A channel is a simple polygon with the start point and goal region consists of a sequence of finite number of adjacent triangles.

It is noted that in a given driving region, there are many channels (Figs. 3*c*–*e*). Considering the actual conditions, the set of safe area provided by one specific channel should be wide enough for the vehicle to pass through. For example, in Figs. 3*c*–*e*, there are three channels P_1, P_2 and P_3 based on the Definition 1. However, there exists some areas which are too narrow for vehicle to overtake in Figs. 3*d* and *e* and thus only channel P_1 is feasible.

Remark 1: A channel is feasible only when all the triangles inside are wide enough for the vehicle to cross. Each feasible channel consists of many possible collision-free paths (e.g. Fig. 3*c*).

Definition 2: The channel P is feasible only if $\forall t_i \in P$ satisfies

$$w_i \le w_v + w_b, \quad \forall i \in 1, \ldots, n \tag{5}$$

where w_v is the vehicle's width while w_b is the buffer width to ensure driver's comfort.

The width w_i of the triangle t_i can be exampled by Fig. 4. The calculation of width is based on the type of triangles as described below.

Type a: The triangle t_i is an acute triangle and shares two vertices with a obstacle/boundary. The driving paths within the triangle t_i has to traverse triangle t_i via its unconstrained edges (A_1A_2 and A_1A_3). In this situation, the 'width' of the triangle t_i can be calculated by

$$w_i = \frac{1}{2}\min\left(\left|A_1A_2\right|, \left|A_1A_1'\right|, \left|A_1A_3\right|\right), \quad i = 1, \ldots, n; \tag{6}$$

where A_1A_1' is an altitude of t_i through the vertex which is opposite its constrained edge and perpendicular to the constrained edge.

Type b: The triangle t_i is an obtuse triangle and shares two vertices with a obstacle/boundary. The driving paths within the triangle t_i has to traverse triangle t_i via its unconstrained edges. The calculation of w_i of t_i is given by

$$w_i = \frac{1}{2}\min\left(\left|A_1A_2\right|, \left|A_1A_3\right|\right), \quad i = 1, \ldots, n; \tag{7}$$

Type c: The vertices of triangle t_i lie on three different obstacles/boundaries, in other words, triangle t_i has no constrained edges. The possible paths enter the triangle t_i via one edge (e.g. A_1A_3) and exit through two possible edges (A_3A_4 and A_1A_4) with two different driving directions. For a given driving direction, the 'width' of the triangle t_i is obtained by the following equation:

$$w_i = \frac{1}{2}\min\left(\left|A_3A_1\right|, \left|A_3A_3'\right|, \left|A_3A_4\right|\right), \quad i = 1, \ldots, n. \tag{8}$$

where vertex A_3 is the intersection point of entering edge and existing edge. The line segment A_3A_3' is an altitude of t_i through vertex A_3 and perpendicular to the opposite side.

The method of feasible channels finding can be summarised in four main steps:

(1) Step 1: For a given driving region, regard other vehicles as polygonal obstacles and discrete the driving region into N constrained Delaunay triangles;

Inputs : Triangles $T_1, \cdots, T_N$
Width of each Triangle $w_i, i = 1, \cdots, N$
X-coordinate of each circumcircle $a_i,\ i = 1, \cdots, N$
Output: $\mathbf{D}$
Initialize: Set $\mathbf{D}$ as a N-by-N matrix of zeros
for $j = 1:1:N$ & $m = 1:1:N$ **do**
  if T_j *and* T_m *is adjacent* **then**
    if $w_j < w_v + w_b$ *and* $w_m < w_v + w_b$ **then**
      $\mathbf{D(j, m)} = \mathbf{1}$
    else
      $\mathbf{D(j, m)} = \mathbf{0}$
    end
  end
end
Return D

Fig. 5 *Algorithm 1: calculation of adjacent matrix* **D**

Inputs : Triangles T_s, T_f
Adjacent matrix $\mathbf{D}$
Output: τ
Initialize: $\tau \leftarrow$ **InitializeTree**(T_s),
Set **SearchEntity**= $\{T_s\}$
while *SearchEntity*$\neq \emptyset$ **do**
  $farnode$=**SearchEntity**(1)
  SearchEntity=SearchEntity-$\{farnode\}$
  SearchEntity= SearchEntity $\cup \mathbf{D}(farnode, :)$
  $Index = find(\mathbf{D}(\text{farnode}, :) == 1)$
  for $i = 1:1:length(Index)$ **do**
    $childnode = T_{Index(i)}$
    $[\tau,\ addnum] \leftarrow$ **InsertTree** $(\tau, farnode, childnode)$
    if $childnode \neq T_f$ & $addnum \geq 1$ & $childnode \notin$ ***SearchEntity*** **then**
      SearchEntity $\leftarrow$ **SearchEntity** $\bigcup$ {childnode}
    end
  end
end

Fig. 6 *Algorithm 2: tree construction*

Inputs : Current tree τ, $farnode$, $childenode$
Output: Newtree, $addnum$
Initialize: $addnum = 0$
$branch \leftarrow$ **FindBranch**$(\tau, farnode)$ % find the branch from the root T_s to the leaf node $farnode$
for *each branch* **do**
  if $childnode \notin branch$ **then**
    add $childenode$ as a child node of $farnode$ in the tree
    $add = 1$
  else
    add T_0 as s a child node of $farnode$ in the tree
    $add = 0$
  end
  $addnum = addnum + add$
end
Return τ and $addnum$

Fig. 7 *Algorithm 3: InsertTree()*

(2) Step 2: Find the triangle $T_s \in \mathcal{T}, 1 \leq s \leq N, \mathcal{T} = \{T_1, T_2, \ldots, T_N\}$ which the starting point S_p belongs and the triangle $T_f \in \mathcal{T}, 1 \leq f \leq N, f \neq s$ which the final point F_p belongs.

(3) Step 3: Construct an adjacent matrix $\mathbf{D}^{N \times N}$ to represent the relationship between any pair of triangles. The calculation of **D** can be summarised as given in Algorithm 1 (see Fig. 5)

(4) Step 4: Based on the adjacent matrix **D**, we create a tree structure in order to find a possible way from T_s to T_f through a sequence of nodes. We set the root as T_s and triangles T_i, $i = 1, \ldots, N, i \neq s$ as nodes. The tree construction can be summarised in Algorithm 2 (see Fig. 6) and the function InsertTree() in Algorithm 2 is described in Algorithm 3 (see Fig. 7).

Based on Algorithms 2 and 3, the τ is a tree structure whose root is T_s and leaf node is either T_0 or T_f. InsertTree() is used to insert a node to the current tree under the father node *farnode* while *branch* is a sequence of nodes from root to *farnode*. Based on τ, we search for feasible channels by finding the branches which starts with T_s and ends with T_f.

Remark 2: If no branch ends by T_f in τ, we search for all the branches staring with T_s and ending at T_0 in order to find branches whose *farnode* of T_0 is close to the T_f. These branches are set as the feasible channels and the *farnodes* of T_0 of these branches are set as T_f. In this way, at least one feasible channel is identified in all the situations at any time step.

After identifying all the feasible channels, the information of each channel should be noticed by the human driver through visual display or auditory signals such that the human driver can make a faster rational decision on the channel. The decision-making problem is solved by TOPSIS algorithm. The TOPSIS is a multi-criteria decision analysis method which ranks the alternatives based on the distance between the alternative and positive/negative ideal solution to obtain the optimal scheme. It has been widely used in path planning, path finding and decision making because of its flexibility, simple computation and rationality [46, 47]. The calculation results of TOPSIS are closely related with the evaluation matrix. We define three metrics, which are 'Length', 'Smoothness' and 'Safety', to evaluate the performance of each channel. Each metric will be explained later in details.

Remark 3: Complexity analysis. In Algorithm 1, the main phase will be repeated for up to $N \times N$ times. Then, the complexity of the Algorithm is $O(N^2)$. In Algorithm 2, the Line 6 can hold up to $2N - 1$ times in the worst case when all the nodes are searched twice excluding T_s. In the for-loop of algorithm, the number of elements in index is at most 2 since one triangle at most has 2 adjacent triangle with a given direction. Then, the complexity of this part is $O(2)$. In terms of function *InsertTree*(), similar with *index*, the complexity is $O(2)$. Therefore, the overall complexity is $O(N^2) + O((2N - 1) \times 2 \times 2) = O(N^2)$.

Assumption 3: We assume that in a given driving region, there are m feasible channels. A feasible channel from $T_s \in \mathcal{T}$ to $T_f \in \mathcal{T}$ is a sequence of triangles $P = (t_1, t_2, \ldots, t_n) \in \mathcal{T} \times \mathcal{T} \times \cdots \times \mathcal{T}, \mathcal{T} = \{T_1, T_2, \ldots, T_N\}$ (where $t_1 = T_s$ and $t_n = T_f$) such that t_i is adjacent to t_{i+1} for $1 \leq i < n$ with a common edge $e_{i,i+1}$ (Fig. 8).

(i) Length: The length is used to describe the average distance travelled by all $t_i \in \mathcal{T}$ for a specific channel (e.g. $P = (t_1, t_2, \ldots, t_n)$) and is calculated by

$$L_P = \sum_{i=1}^{n} L_{i,i+1} \tag{9}$$

where $M_{i-1,i}$ is the midpoint on the edge $e_{i-1,i}$ and $L_{i-1,i}$ is the length connecting $M_{i-2,i-1}$ with $M_{i-1,i}$ (Fig. 9).

(ii) Smoothness: Similar with turn number, the path generated in the channel P is required to be as smooth as possible by considering the driving comfort. The angle of the line segment is used to describe the smoothness of the triangles (Fig. 9), i.e.

$$S_P = \sum_{i=1}^{n} \phi_{i-1,i} \tag{10}$$

(iii) Safty: The safety is used to describe the 'width' of the channel and has been introduced before. It is noted that the wider the channel is, the less driving skill is required and the safer the channel is. The safety of a specific channel is calculated as

$$S_s = \sum_{i=1}^{n-1} \frac{1}{\min(w_i, w_{i+1})} \tag{11}$$

By identifying the metrics, the following algorithm describes the TOPSIS method:

(1) Step 1: Construct the evaluation matrix $\mathbf{A}^{m*3} = (a_{ij})_{m\times n}$ based on m feasible channels and $n = 3$ attributes (length, smoothness and safety),

(2) Step 2; Determine the weights $\mathbf{W} = (w_j)_{1\times n}$ of attributes based on the human driver's preference. For example, if the driver prefers to achieve the destination as soon as possible, the weight of the length should be larger than the others,

(3) Step 3: Normalise matrix $\mathbf{A}$ and get $\mathbf{R} = (r_{ij})_{m\times n}$, $r_{ij} = a_{ij}/\sqrt{\sum_{k=1}^{m} a_{kj}^2}$. Calculate the weighted normalised decision matrix $\mathbf{T} = (t_{ij}) = r_{ij} \cdot w_j$, $i = 1, 2, \ldots, m$, $j = 1, \ldots, n$,

(4) Step 4: Determine the target distance d_i^+ between the alternative i and the best condition A^+

$$\begin{aligned} d_i^+ &= \sqrt{\sum_{j=1}^{n} (t_{ij} - t_j^+)^2}, \\ A^+ &= \{(\max_i t_{ij} \,|\, j \in J^+), (\min_i t_{ij} \,|\, j \in J_\star)\} \\ &= \{t_j^+ \,|\, j = 1, 2, \ldots, n\} \end{aligned} \tag{12}$$

where $J^+ = \{j = 1, 2, \ldots, n \,|\, j\}$ is a set with positive attributes.

Determine the target distance d_i^- between the alternative i and the worst condition A^-

$$\begin{aligned} d_i^- &= \sqrt{\sum_{j=1}^{n} (t_{ij} - t_j^-)^2}, \\ A^- &= \{(\min_i t_{ij} \,|\, j \in J^+), (\max_i t_{ij} \,|\, j \in J^-)\} \\ &= \{t_j^- \,|\, j = 1, 2, \ldots, n\} \end{aligned} \tag{13}$$

where $J^- = \{j = 1, 2, \ldots, n \,|\, j\}$ is a set with positive attributes.

(5) Step 5: Calculating coefficients $H_i^\star$ based on the following equation:

$$H_i^\star = \frac{J_i^-}{J_i^- + J_i^+}, 0 \le H^\star \le 1 \tag{14}$$

(6) Step 6: Rank the alternatives based on $H_i^\star$.

Once the optimal channel $P_\star$ (rank one) is identified, the physical positions of its edges can be enforced as position constraints of the ego vehicle which can be compactly written as the following linear inequality:

$$y_{\min}(k) + d_b \le Y(k) \le y_{\max}(k) - d_b \tag{15}$$

where $y_{\min}$ and $y_{\max}$ represent the lower and upper bound of ego vehicle's position at each time step k, respectively, and d_b is a minimum safe distance between obstacle/boundary and ego vehicle to ensure driving comfort. Equation (15) is compactly written as

$$L(x, u) \le \mathbf{0} \tag{16}$$

3.2.2 Time to collision: In this section, we introduce TTC as a decision-making aid to avoid the longitudinal collisions. TTC is firstly suggested by Hayward in 1972 [48] and has proven to be an effective measure for traffic safety analyses. In our paper, we redefine the TTC as follows:

Definition 3: TTC is the time that the ego vehicle will have a longitudinal collision with another vehicle in its immediate vicinity if the present trajectories continue to be followed.

By introducing position constraints in the definition of TTC, the calculation of TTC allows the ego vehicle to change the lane ahead of time. The TTC is computed every time step for ego vehicle based on its prediction position and current velocity

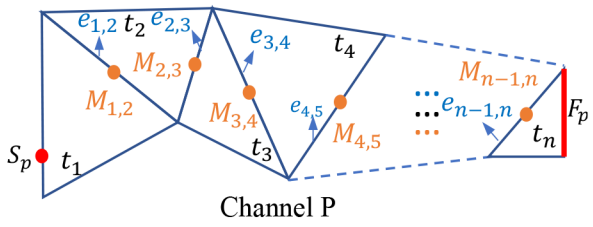

Fig. 8 *Illustration of a feasible channel P*

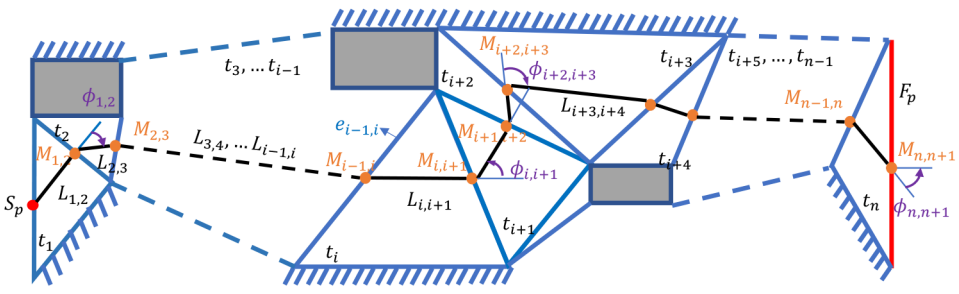

Fig. 9 *Illustration of length of Channel P*

$$\mathrm{TTC} = \frac{d_\mathrm{r}}{v_x} \tag{17}$$

where d_r is the relative distance between predicted position of ego vehicle and forward obstacle/vehicle in longitudinal direction and v_x is the current vehicle's velocity. It should be mentioned that the TTC must satisfy

$$\mathrm{TTC} \geq \text{minimum TTC} \tag{18}$$

The value of minimum TTC depends on the driving scenario, vehicle's velocity, acceleration and so on. The larger the value of minimum TTC is, the more intense actions should be applied and vice versa. Constraint (18) can be rewritten as

$$T(x, u) \leq \mathbf{0}. \tag{19}$$

3.3 Stability constraints

In this paper, the vehicle stability is guaranteed through constraints on the maximum front tyre slip angle and yaw rate [33]. By neglecting the effects of weight transfer and assuming zero longitudinal tyre forces, the bounds of yaw rate can be identified as

$$r_\mathrm{max} = \frac{g\mu}{v_x} \tag{20}$$

where g is the gravitational constant and μ is the surface coefficient of friction.

Another important consideration for vehicle stability is the sideslip. Based on [35] ,the maximum sideslip β can be represented as

$$\beta \simeq \tan\frac{v_y}{v_x} \leq \beta_\mathrm{max} = \tan^{-1}\left(3\frac{mg\mu}{C_\mathrm{r}}\frac{l_\mathrm{f}}{l_\mathrm{f}+l_\mathrm{r}}\right) + \frac{l_\mathrm{r} r}{v_x} \tag{21}$$

In summary, the constraints (21) and (20) can be compactly written as

$$S(x, u) \leq \mathbf{0}. \tag{22}$$

3.4 Feasibility constraints

Since the vehicle consists of many complicated mechanical systems, it subjects to limitations which are related to the physical properties of the vehicle. In general, the maximum front wheel angle depends on the available wheel-well space and is constrained by the mechanical linkages between each wheel. The front wheel angle for a traditional front wheel steering vehicle is usually between −35° and 35° and between −90° and 90° in the four-wheel independently steering system [41]. In this paper, we assume T_a satisfies

$$\delta_\mathrm{amin} \leq \delta_\mathrm{a} \leq \delta_\mathrm{amax} \tag{23}$$

In addition, the brake torque applied by automation is modulated between the maximum and minimum torque, i.e.

$$T_\mathrm{amin} \leq T_\mathrm{a} \leq T_\mathrm{amax}, \tag{24}$$

Furthermore, the vehicle's operation should meet the requirements of driving comfort which can effectively prevent frequent accelerating/decelerating or steering. By considering the passenger's comfort

$$\begin{aligned} \Delta\delta_\mathrm{amin} \leq \Delta\delta_\mathrm{a} \leq \Delta\delta_\mathrm{amax}, \\ \Delta T_\mathrm{amin} \leq \Delta T_\mathrm{a} \leq \Delta T_\mathrm{amax}. \end{aligned} \tag{25}$$

where δ_amin, δ_amax, ΔT_amin and ΔT_amax denote the saturation level, respectively.

4 MPC-based shared controller design

Here, we introduce a reference-free shared control system for autonomous driving. Based on the driving environmental information and driving task requirement, the driver operates the vehicle in order to achieve the driving goal (e.g. lane-change or overtaking the forward vehicle). As mentioned before, the input signals of vehicle are driver-commanded steering angle δ_f and corrected steering angle δ_a. The automation continuously monitors the vehicle's states and evaluates the driver's actions. Once the vehicle's predicted states are against the safety constraints introduced in Section 3.2, a corrected steering angle δ_a and acceleration/brake torque T_a are generated by MPC algorithm and implemented to the vehicle to guarantee the safety of vehicle.

We discretise system (4) with fixed sampling time T_p to obtain

$$x_{k+1} = f^d(x_k, u_k) \tag{26}$$

The optimisation problem under investigation is formulated as follows:

$$\min_{\mathscr{U}_t, \epsilon} \sum_{k=0}^{H_\mathrm{c}-1} \|u_{t+k,t}\|_Q^2 + \|\Delta u_{t+k,t}\|_R^2 + \rho\epsilon \tag{27a}$$

$$s.t.\ \ x_{t+k+1,t} = f^d(x_{t+k,t}, u_{t+k,t}), \quad k = 0, \ldots, H_\mathrm{p}-1 \tag{27b}$$

$$u_{t+k,t} = \Delta u_{t+k,t} + u_{t+k-1,t} \tag{27c}$$

$$u_\mathrm{min} \leq u_{t+k,t} \leq u_\mathrm{max}, \quad k = 0, \ldots, H_\mathrm{c}-1 \tag{27d}$$

$$\Delta u_\mathrm{min} \leq \Delta u_{t+k,t} \leq \Delta u_\mathrm{max}, \quad k = 0, \ldots, H_\mathrm{c}-1 \tag{27e}$$

$$L_t(x_{t+k,t}, u_{t+k,t}) \leq 1\epsilon, \quad k = 0, \ldots, H_\mathrm{p}, \epsilon \geq 0 \tag{27f}$$

$$T_t(x_{t+k,t}, u_{t+k,t}) \leq 1\epsilon, \quad k = 0, \ldots, , H_\mathrm{p}, \epsilon \geq 0 \tag{27g}$$

$$S_t(x_{t+k,t}, u_{t+k,t}) \leq 1\epsilon, \quad k = 0, \ldots, , H_\mathrm{p}, \epsilon \geq 0 \tag{27h}$$

$$\Delta u_{t+k,t} = 0, \quad k = H_\mathrm{c}, \ldots, H_\mathrm{p} \tag{27i}$$

$$u_{t-1,t} = u(t-1) \tag{27j}$$

$$x_{t,t} = x(t) \tag{27k}$$

where t denotes the current time step and and $x_{t+k,t}$ denotes the predicted state at time $t+k$ obtained by applying control sequence $\mathscr{U}_t = [u_{t,t}, \ldots, u_{t+k,t}]$ to system (26) with $x_{t,t} = x(t)$. Q, R and ρ are weight factors of control actions, change rate of control and violation of soft constraints, respectively. H_c is the control horizon while H_p is the prediction horizon with $H_\mathrm{p} \geq H_\mathrm{c}$. The control inputs are $u = [\delta_\mathrm{a}, T_\mathrm{a}]$, $u_\mathrm{min} = [\delta_\mathrm{amin} \quad T_\mathrm{amin}]^\mathrm{T}$ and $u_\mathrm{max} = [\delta_\mathrm{amax} \quad T_\mathrm{amax}]^\mathrm{T}$. $\Delta u = [\Delta\delta_\mathrm{a}, \Delta T_\mathrm{a}]^\mathrm{T}$, $\Delta u_\mathrm{min} = [\Delta\delta_\mathrm{amin} \quad \Delta T_\mathrm{amin}]^\mathrm{T}$ and $\Delta u_\mathrm{max} = [\Delta\delta_\mathrm{amax} \quad \Delta T_\mathrm{amax}]^\mathrm{T}$.

Remark 4: It should be mentioned that there is no reference path/trajectory imposed in cost function (27a). The objective of optimisation problem is to minimise control action without violating the safety constraints (27d)–(27h). If the driver is capable of steering the vehicle with driver-commanded steering angle δ_f, no corrective control action will be applied ($\delta_\mathrm{a} = 0$) and the cost function will thus be zero. On the contrary, if the driver cannot handle the driving situation and violate any constraints of (27d)–(27h), a corrective control action is generated by the optimisation problem (27a) and implemented to the vehicle.

Remark 5: The problem formulation in (27) is a non-linear receding horizon optimisation problem with linear inequality constraints (27d)–(27e) and non-linear inequality constraints (27f)–(27h) with initial status (27j)–(27k). The above optimisation

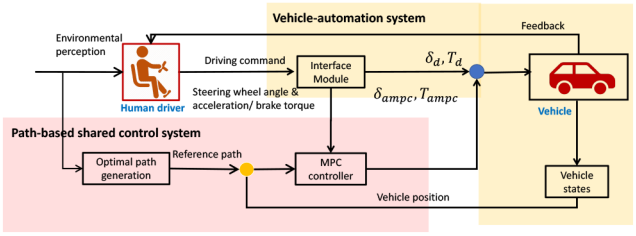

Fig. 10 *Path-based shared control system with MPC controller*

Table 1 Vehicle parameters

Parameter	Value
l_f	1.21 m
l_r	1.05 m
m	2000 kg
I_Z	1300 kg · m^2
μ	0.5
$C_{\alpha f}$	30000N/unit slip ratio
$C_{\alpha r}$	20000N/unit slip ratio

problem can be effectively solved by *fmincon* in MATLAB simulation environment.

Remark 6: (27b) represents the vehicle dynamics with a given driver's command δ_d. The non-linear constraints (27f)–(27h) reflect position constraints, TTC limitations and stability constraints, respectively. In addition, a slack variable ϵ is introduced to soft the non-linear constraints. The hard constraints (27d)–(27e) are imposed to set the limitations on the control actions $[\delta_a\ T_a]^T$.

5 Simulation validation

In this section, we conduct series of simulation studies aiming to answer the following research questions:

RQ1: *Can our approach ensure the vehicle drives safely?*
RQ2: *Can our approach mitigate human–machine conflicts compared with path-based approaches?*
RQ3: *What factors can influence the performance of our approach?*

Here, the exploration of RQ1 aims to demonstrate the efficiency of introducing safety constraints in our paper. Furthermore, to concern RQ2, we give the following definition of *conflict* in path-based approaches.

Definition 4: Conflict occurs if there is a difference between human driver's expectations and automated planning results. In a given task, the more times the conflict occurs, the more severe it is.

This is to say, if the driver's behaviours cannot meet the automated planning results (optimal path), there is a human–machine conflict. In the path-based approach, if a conflict occurs, automation then assists the driver to follow the optimal path in order to eliminate the conflict. By evaluating the occurrence of conflicts, we can further identify the superiority of proposed reference-based approach. Finally, concerning RQ3, we explore some factors (such as minimum TTC, H_p) that can influence the occurrence of conflicts and computation time of our approach.

5.1 Path-based MPC shared control system

To compare with our approach, we design a path-based shared control system based on MPC (Fig. 10) where the optimal path is generated based on Dubins method [49]. Dubins path is proven to be shortest and flexible, consisting of circular arcs and straight line segments. The aim of the MPC controller is to keep the vehicle following the optimal path. The outputs of the MPC controller ($[\delta_{ampc}\ T_{ampc}]^T$) are the assisted steering wheel angle and acceleration/brake torque which will be implemented to the vehicle together with the driver's commands. More details can be found in [50].

5.2 Simulation environment

The simulation environment is set as follows:

(i) The front wheel angles of automation lie only within $-30°$ to $30°$. If an input angle outside of its range is entered, the vehicle will not be able to turn to that amount. The braking torque of automation is bounded in $[-20, 50](\mathrm{N}\cdot\mathrm{m})$.
(ii) The limitations on changes of control actions are set as

$$-20\times\frac{\pi}{180}\le\delta_a(\delta_{ampc})\le 20\times\frac{\pi}{180}$$
$$-20\le T_a(T_{ampc})\le 20$$

(iii) The sample time is 0.1 s. The control horizon is $H_c = 5$ while prediction horizon is $H_p = 10$.
(iv) The minimum TTC is set as 0.35 s.
(v) The minimum safe distance $d_b = 1$ m
(vi) The parameters of vehicle are given by Table 1.

5.3 Driving scenario set up

We consider two different driving scenarios including a two-way road (Fig. 11) and a three lane highway (Fig. 12). The road width is 3.5 m. The ego vehicle drives from the start position $(0, 0)$. In the two-way road, the initial speed of the ego vehicle is 15 while 10 m/s in three lane highway. The other vehicles (Vehicle Blue, Pink, Yellow and so on) are assumed to drive in their initial lanes and the width of each vehicle is between [2 ,2.5]m. The speed of each vehicle are assumed to be measured by the sensors

$$v_{\text{Vehicle Blue}} = 8\,\text{m/s},\ v_{\text{Vehicle Red}} = 10\,\text{m/s},$$
$$v_{\text{Vehicle Pink}} = 10\,\text{m/s},\ v_{\text{Vehicle Black}} = 10\,\text{m/s},$$
$$v_{\text{Vehicle Yellow}} = 15\,\text{m/s},\ v_{\text{Vehicle Orange}} = 10\,\text{m/s},$$
$$v_{\text{Vehicle Greed}} = 10\,\text{m/s},\ v_{\text{Vehicle Grey}} = 10\,\text{m/s}.$$

5.4 Simulation results and analysis

5.4.1 RQ1-Can our approach ensure the vehicle drives safely?: Fig. 13 shows the comparison results between the proposed approach and path-based approach in two-way road and three lane highway, respectively. Fig. 13*a* shows the driving performance of path-based approach and proposed reference-free

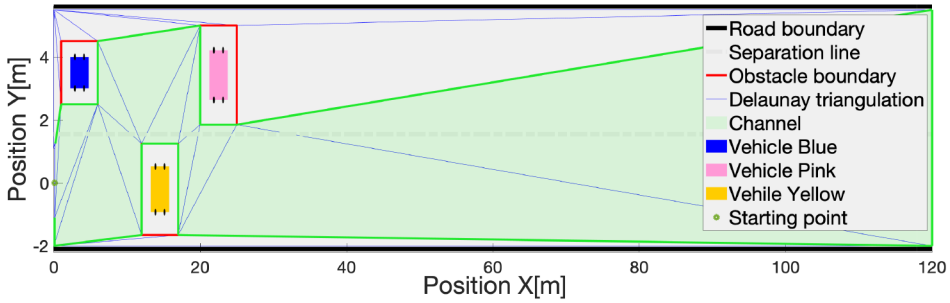

Fig. 11 *Driving performance in two-way road*

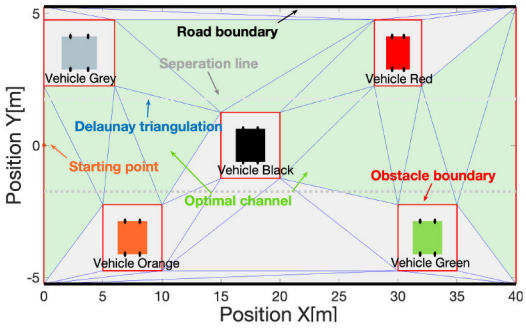

Fig. 12 *Three lane driving scenario*

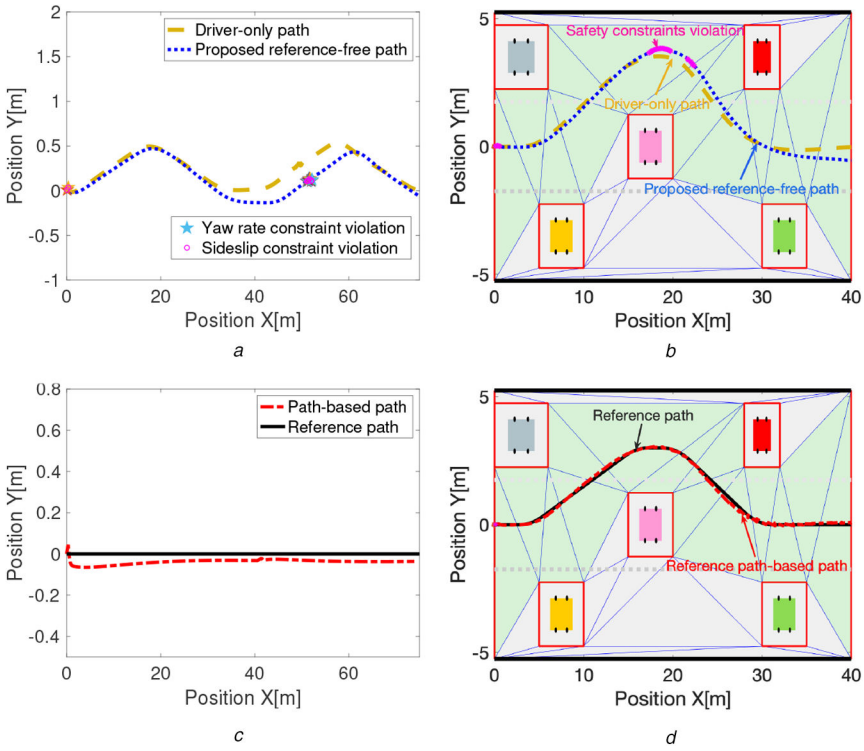

Fig. 13 *Comparison results between the proposed approach and path-based approach*

(a) Driving performance of proposed approach in three lane scenario, ***(b)*** Driving performance of proposed approach in three lane highway, ***(c)*** Driving performance of path-based approach in two-way road, ***(d)*** Driving performance of path-based approach in three lane highway

approach and Fig. 14 shows the identification of channels at each time. Fig. 13*b* represents the driving performance in three lane highway. Particularly, we assume the driver more cares about the safety and path length. Then the weights mentioned in Section (2) are given by

$$\mathbf{W} = \begin{bmatrix} w_{\text{length}} & w_{\text{smoothness}} & w_{\text{safety}} \end{bmatrix} = [5, 1, 4]\,.$$

An optimal channel is selected by the TOPSIS algorithm and shown as green area in Figs. 14 and 13*b*. The yellow dotted line represents the path generated by the given driver's inputs with no automation. The proposed reference-free approach can provide a collision-free path (blue dash line) without knowing the reference path. It is shown that the optimal channel can guarantee a safe area for vehicle where no potential collisions will occur at any time step (Fig. 14) and the automation only corrects the driver's inputs by implementing corrective actions into the vehicle when the safety constraints are violated.

Remark 7: Without having a given optimal/reference path to follow, our approach can allow the driver to execute different tasks based on his or her operational preference, such as change the lane, follow the front vehicle or overtake the front vehicle. In this way,

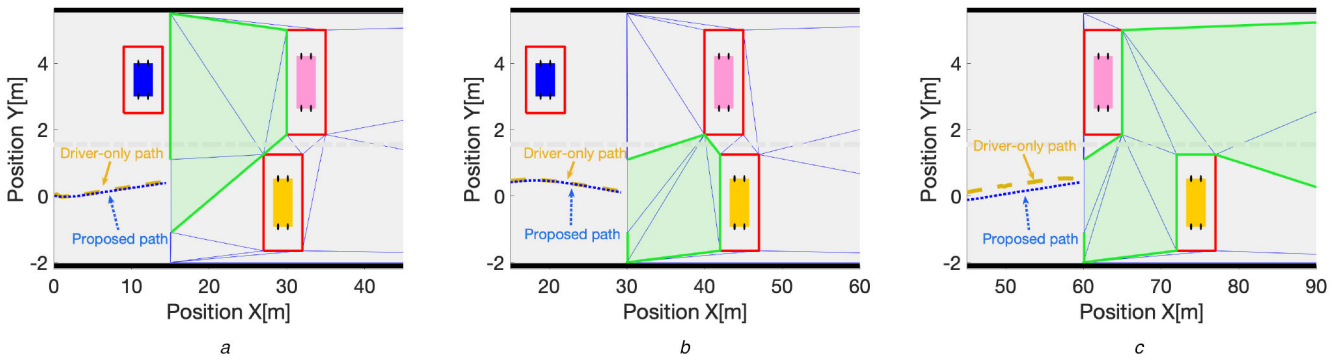

Fig. 14 *Driving performance in two-lane driving scenario*
(a) t=1 s, ***(b)*** t=2 s, ***(c)*** t=4 s

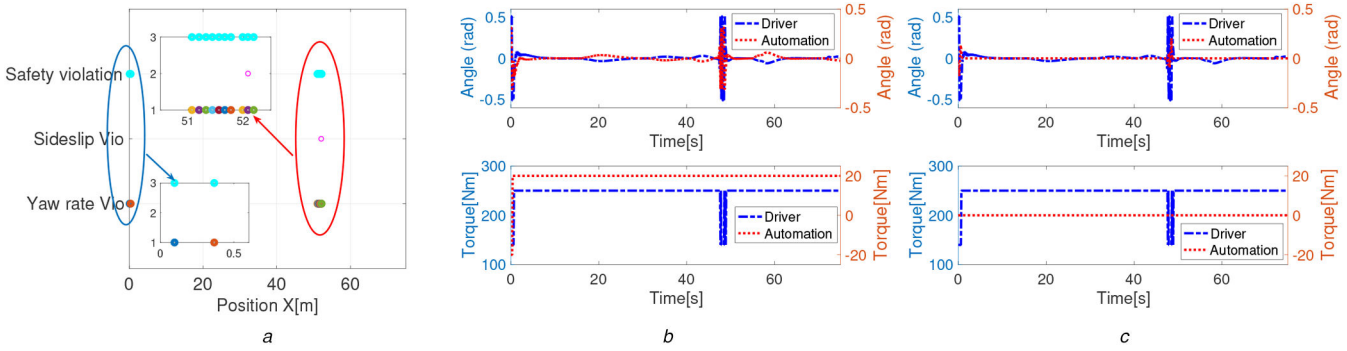

Fig. 15 *Occurrence of conflicts in two-way road*
(a) Number of conflicts in two-way road, ***(b)*** Automation actions of path-based approach, ***(c)*** Automation actions of proposed approach

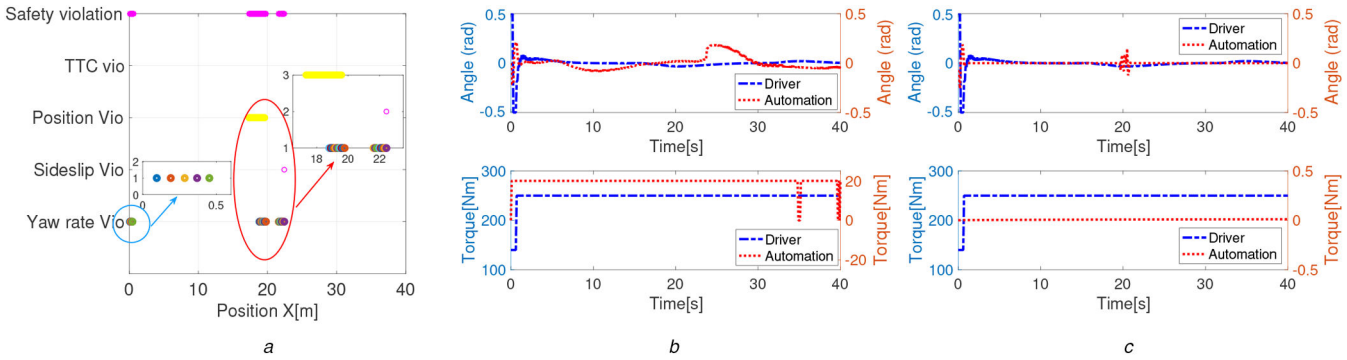

Fig. 16 *Occurrence of conflicts in three-lane road*
(a) Number of conflicts in three lane highway, ***(b)*** Automation actions of path-based approach, ***(c)*** Automation actions of proposed approach

our approach can offer the driver the authority of the vehicle control to the maximum extent.

5.4.2 RQ2-Can our approach mitigate human–machine conflicts compared with path-based approach?: To better answer RQ2, we utilise the path-based shared control system designed in Section 5.1 to generate reference path and path-based path, respectively. We assume that in the two-way road, the ego vehicle is required to follow the front vehicle and drives close to the centreline of the current lane. In the three lane driving scenario, the human driver would like to overtake the front vehicle (Vehicle Black) on the premise of safety. The reference path of both driving scenarios are shown in Figs. 13*c* and *d* with black solid line, respectively. The red dash dot line represents the driving path generated by the path-based approach considering the given driver inputs (blue dash-dot line in Figs. 15*b*,*c* and Figs. 16*b*, *c*). It is shown that the MPC controller designed in Section 5.1 can allow the vehicle to accurately follow the reference path.

In addition, we further observe the occurrence of conflict in path-based approach and proposed approach and plot the control actions of both approaches as well.

The assisted control actions ($[\delta_{\text{ampc}}\, T_{\text{ampc}}]^{\text{T}}$) generated from the automation are shown in Figs. 15*b* and 16*b*. It is shown that in order to keep the vehicle following the reference path, the automation has to continuously implement the assisted control actions to the vehicle. The human–machine conflict always occurs during the driving operation. By contrast, our approach allows the automaton to implement the corrected control actions ($[\delta_a\, T_a]^{\text{T}}$) only when the safety constraints are violated. It is also found the conflict in proposed approach only occurs at [0 0.5] m and [51 53]m, and only sideslip angle and yaw rate constraints violation are triggered in two-way driving scenario (Fig. 15*a*). In the three lane driving scenario, the conflicts mainly occur at the beginning and around 22 m when the vehicle drives the second turn. In summary, the proposed approach can mitigate human machine conflicts and offer the driver as much freedom as possible.

5.4.3 RQ3-What factors can influence the performance of our approach?: Since there are not many conflicts happened in two-way driving scenario, we only consider the impact of H_{p}, d_b and minimun TTC on the performance of the proposed approach, specially in three lane driving scenario.

From Tables 2–4, it is shown once the prediction horizon H_{p} is increased, the number of the conflicts is reduced. It is because once the prediction horizon increases, the earlier the automation take

Table 2 Impact of H_p on number of conflicts

	Num of conflicts with min TTC=0.5 and $d_b = 1.5$			
	$H_p = 1$	$H_p = 10$	$H_p = 20$	$H_p = 30$
Num	39	22	10	24

Table 3 Impact of minmum TTC on number of conflicts

	Num of conflicts with $H_p = 10$ and $d_b = 1.5$			
	min TTC=0.35	0.75	1	1.2
Num	17	43	50	219

Table 4 Impact of d_b on number of conflicts

	Num of conflicts with min TTC=0.5 and $H_p = 10$			
	$d_b = 1.2$	$d_b = 1.5$	$d_b = 2$	$d_b = 2.2$
Num	17	22	42	50

actions and the better the driving performance is. However, a big prediction horizon may place computational burden and increase computation time. $H_p = 20$ is the optimal setting in three lane driving scenario based on Table 2.

Based on Table 3, we notice that with the increase of minimum TTC, the automation can detect the head-on obstacle more timely and execute an appropriate control action immediately. However, a big minimum TTC may result in that the automation frequently intervenes and therefore over restricts the driver's freedom. Thus, the selection of minimum TTC depends on the preferences or needs (comfort, speed, safety) and driver's skill.

The parameters which relate to the soft constrains such as d_b should be designed based on the driving scenario and driver's preferences (Table 4). A more strict constraint may cause continuously corrections and lead to a conflict between driver and automation. A less strict constraint may lead to a condition that there is no feasible solution of optimisation problem (27) and the automation cannot handle. Therefore, these parameters have significantly impact on the performance and computational efficiency of the proposed approach. The further study will be conducted on the identification of these parameters on an experimental platform.

6 Conclusion

In this paper, a novel reference-free framework for the shared control system of automated vehicles is designed. Without requirement of a reference path, we place limitations on the vehicle's status in terms of driving performance, safety and stability. In this way, the automation shares the control authority with the human driver in a harmonic manner with less interventions to mitigate human–machine conflicts. More specifically, the automation system allows the human driver to dominate the control authority within safe corridors, and it would only intervene the control to avoid collisions in risky conditions. The system models, safety constraints and the proposed shared controller are developed, integrated and tested in simulations. The results show that the proposed approach is able to ensure the safety and stability of the system under risky driving conditions. Moreover, it can effectively mitigate human–machine conflicts during shared control tasks, compared to an existing approach, validating its feasibility and effectiveness. Further work includes deeper analysis of parameters of soft constraints, and comprehensive testing and evaluation of the proposed approach on experimental platform.

7 Acknowledgment

This work was supported in part by the SUG-NAP Grant (no. M4082268.050) of Nanyang Technological University, Singapore, and A*STAR Grant (no. 1922500046), Singapore.

8 References

[1] Li, W., Xie, Z., Wong, P.K., *et al.*: 'Adaptive-event-trigger-based fuzzy nonlinear lateral dynamic control for autonomous electric vehicles under insecure communication networks', *IEEE Trans. Ind. Electron.*, 2020

[2] Hu, C., Wang, Z., Taghavifar, H., *et al.*: 'Mme-ekf-based path-tracking control of autonomous vehicles considering input saturation', *IEEE Trans. Veh. Technol.*, 2019, **68**, (6), pp. 5246–5259

[3] Xing, Y., Lv, C., Cao, D., *et al.*: 'Energy oriented driving behavior analysis and personalized prediction of vehicle states with joint time series modeling', *Appl. Energy*, 2020, **261**, p. 114471

[4] Xing, Y., Lv, C., Cao, D.: 'Personalized vehicle trajectory prediction based on joint time series modeling for connected vehicles', *IEEE Trans. Veh. Technol.*, 2019, **69**, pp. 1341–1352

[5] Liu, Y., Zhang, H.: 'Robust driver-automation shared control for a lane keeping system using interval type 2 fuzzy method'. 2019 IEEE 28th Int. Symp. on Industrial Electronics (ISIE), Vancouver, Canada, 2019, pp. 1944–1949

[6] Huang, C., Naghdy, F., Du, H., *et al.*: 'Review on human-machine shared control system of automated vehicles'. 2019 3rd Int. Symp. on Autonomous Systems (ISAS), Shanghai, China, 2019, pp. 47–51

[7] Lu, Z., Happee, R., Cabrall, C.D., *et al.*: 'Human factors of transitions in automated driving: a general framework and literature survey', *Transp. Res. F: Traffic Psychol. Behaviour*, 2016, **43**, pp. 183–198

[8] Litman, T.: 'Autonomous vehicle implementation predictions'. Victoria Transport Policy Institute, Victoria, Canada, 2017

[9] Huang, C., Naghdy, F., Du, H., *et al.*: 'Shared control of highly automated vehicles using steer-by-wire systems', *IEEE/CAA J. Autom. Sinica*, 2019, **6**, (2), pp. 410–423

[10] Anderson, S.J., Walker, J.M., Iagnemma, K.: 'Experimental performance analysis of a homotopy-based shared autonomy framework', *IEEE Trans. Human-Machine Syst.*, 2014, **44**, (2), pp. 190–199

[11] Griffiths, P.G., Gillespie, R.B.: 'Sharing control between humans and automation using haptic interface: primary and secondary task performance benefits', *Hum. Factors*, 2005, **47**, (3), pp. 574–590

[12] Goodrich, K., Williams, R., Schutte, P.: 'Piloted evaluation of the h-mode, a variable autonomy control system, in motion-based simulation'. AIAA Atmospheric Flight Mechanics Conf. and Exhibit, Honolulu, Hawaii, 2008, p. 6554

[13] Kragic, D., Marayong, P., Li, M., *et al.*: 'Human-machine collaborative systems for microsurgical applications', *Int. J. Robot. Res.*, 2005, **24**, (9), pp. 731–741

[14] Muslim, H., Itoh, M.: 'Haptic shared guidance and automatic cooperative control assistance system: performance evaluation for collision avoidance during hazardous lane changes', *SICE J. Control, Meas. Syst. Integr.*, 2017, **10**, (5), pp. 460–467

[15] Bengler, K., Zimmermann, M., Bortot, D., *et al.*: 'Interaction principles for cooperative human-machine systems', *it-Information Technology Methoden und innovative Anwendungen der Informatik und Informationstechnik*, 2012, **54**, (4), pp. 157–164

[16] Mulder, M., Abbink, D.A., Boer, E.R.: 'Sharing control with haptics: seamless driver support from manual to automatic control', *Hum. Factors*, 2012, **54**, (5), pp. 786–798

[17] Nishimura, R., Wada, T., Sugiyama, S.: 'Haptic shared control in steering operation based on cooperative status between a driver and a driver assistance system', *J. Human-Robot Inter.*, 2015, **4**, (3), pp. 19–37

[18] Shakhovska, N.: '*Advances in intelligent systems and computing*' (Springer, Lviv, Ukraine, 2017)

[19] Spence, C., Ho, C.: 'Tactile and multisensory spatial warning signals for drivers', *IEEE Trans. Haptics*, 2008, **1**, (2), pp. 121–129

[20] Steele, M., Gillespie, R.B.: 'Shared control between human and machine: using a haptic steering wheel to aid in land vehicle guidance', *Proc. Human Factors Ergonomics Soc. Ann. Meeting*, 2001, **45**, (23), pp. 1671–1675

[21] Liang, Z., Zhao, J., Dong, Z., *et al.*: 'Torque vectoring and rear-wheel-steering control for vehicle's uncertain slips on soft and slope terrain using sliding mode algorithm', *IEEE Trans. Veh. Technol.*, 2020, **69**, (4), pp. 3805–3815

[22] Mulder, M., Mulder, M., Van Paassen, M., *et al.*: 'Haptic gas pedal feedback', *Ergonomics*, 2008, **51**, (11), pp. 1710–1720

[23] Mulder, M., Mulder, M., van Paassen, M., *et al.*: 'Car-following support with haptic gas pedal feedback'. Proc. of IFAC Symp. on Analysis, Design, and Evaluation of Human-Machine Systems, Georgia, USA., 2004

[24] Mulder, M., Kitazaki, S., Hijikata, S., *et al.*: 'Reaction-time task during car-following with an active gas pedal'. 2004 IEEE Int. Conf. on Systems, Man and Cybernetics (IEEE Cat. No. 04CH37583), Washington, D.C., USA., 2004, vol. 3, pp. 2465–2470

[25] Wada, T., Sonoda, K., Okasaka, T., *et al.*: 'Authority transfer method from automated to manual driving via haptic shared control'. 2016 IEEE Int. Conf. on Systems, Man, and Cybernetics (SMC), Budapest, Hungary, 2016, pp. 002659–002664

[26] Saleh, L., Chevrel, P., Claveau, F., *et al.*: 'Shared steering control between a driver and an automation: stability in the presence of driver behavior uncertainty', *IEEE Trans. Intell. Transp. Syst.*, 2013, **14**, (2), pp. 974–983

[27] Guo, C., Sentouh, C., Popieul, J.-C., *et al.*: 'Predictive shared steering control for driver override in automated driving: a simulator study', *Transp. Res. F: Traffic Psychol. Behaviour*, 2019, **61**, pp. 326–336

[28] Inoue, S., Ozawa, T., Inoue, H., *et al.*: 'Cooperative lateral control between driver and adas by haptic shared control using steering torque assistance combined with direct yaw moment control'. 2016 IEEE 19th Int. Conf. on Intelligent Transportation Systems (ITSC), Rio de Janeiro, Brazil, 2016, pp. 316–321

[29] Carsten, O., Martens, M.H.: 'How can humans understand their automated cars? hmi principles, problems and solutions', *Cogn. Technol. Work*, 2019, **21**, (1), pp. 3–20
[30] Lu, Y., Bi, L., Li, H.: 'Model predictive-based shared control for brain-controlled driving', *IEEE Trans. Intell. Transp. Syst.*, 2020, **21**, (2), pp. 630–640
[31] Chen, Y., He, H., An, X.: 'Motion planning of intelligent vehicles: a survey'. 2006 IEEE Int. Conf. on Vehicular Electronics and Safety, Shanghai, China, 2006, pp. 333–336
[32] Ma, L., Yang, J., Zhang, M.: 'A two-level path planning method for on-road autonomous driving'. 2012 Second Int. Conf. on Intelligent System Design and Engineering Application, Sanya, China, 2012, pp. 661–664
[33] Erlien, S.M.: 'Shared vehicle control using safe driving envelopes for obstacle avoidance and stability'. Ph.D. dissertation, Stanford University, 2015
[34] Gray, A., Ali, M., Gao, Y.*, et al.*: 'A unified approach to threat assessment and control for automotive active safety', *IEEE Trans. Intell. Transp. Syst.*, 2013, **14**, (3), pp. 1490–1499
[35] Erlien, S.M., Fujita, S., Gerdes, J.C.: 'Safe driving envelopes for shared control of ground vehicles', *IFAC Proc. Volumes*, 2013, **46**, (21), pp. 831–836
[36] Sentouh, C., Nguyen, A.-T., Benloucif, M.A.*, et al.*: 'Driver-automation cooperation oriented approach for shared control of lane keeping assist systems', *IEEE Trans. Control Syst. Technol.*, 2018, **27**, (5), pp. 1962–1978
[37] Petermeijer, S.M., Abbink, D.A., Mulder, M.*, et al.*: 'The effect of haptic support systems on driver performance: a literature survey', *IEEE Trans. Haptics*, 2015, **8**, (4), pp. 467–479
[38] Blanco, M., Atwood, J., Vasquez, H.M.*, et al.*: 'Human factors evaluation of level 2 and level 3 automated driving concepts'. Tech. Rep., 2015
[39] Lotz, F.: 'System architectures for automated vehicle guidance concepts', in '*Automotive systems engineering*' (Springer, Berlin, Heidelberg, 2013), pp. 39–61
[40] Anderson, S.J., Karumanchi, S.B., Iagnemma, K.: 'Constraint-based planning and control for safe, semi-autonomous operation of vehicles'. 2012 IEEE Intelligent Vehicles Symp., Alcala de Henares, Spain, June 2012, pp. 383–388
[41] Rajamani, R.: '*Vehicle dynamics and control*' (Springer Science & Business Media, Boston, MA, USA., 2011)
[42] Ito, K.: 'Vehicle control system for controlling side slip angle and yaw rate gain'. uS Patent 4,767,588, 30 August 1988
[43] Cao, C.: 'Topological path planning for crowd navigation'. Ph.D. dissertation, Carnegie Mellon University Pittsburgh, 2019
[44] Demyen, D., Buro, M.: 'Efficient triangulation-based pathfinding', *Aaai*, 2006, **6**, pp. 942–947
[45] Yan, H., Wang, H., Chen, Y.*, et al.*: 'Path planning based on constrained delaunay triangulation'. 2008 7th World Congress on Intelligent Control and Automation, Chongqing, China, 2008, pp. 5168–5173
[46] Roszkowska, E.: 'Multi-criteria decision making models by applying the topsis method to crisp and interval data', *Multiple Criteria Decision Making/ University of Economics in Katowice*, 2011, **6**, pp. 200–230
[47] Zhou, J., Zheng, H., Wang, J.*, et al.*: 'Multi-objective optimization of lane-changing strategy for intelligent vehicles in complex driving environments', *IEEE Trans. Veh. Technol.*, 2019, **69**, pp. 1291–1308
[48] Hayward, J.C.: 'Near miss determination through use of a scale of danger', 1972
[49] Bevan, G.P.: 'Development of a vehicle dynamics controller for obstacle avoidance'. Ph.D. dissertation, University of Glasgow, 2008
[50] Huang, C., Li, B., Kishida, M.: 'Model predictive approach to integrated path planning and tracking for autonomous vehicles'. 2019 IEEE Intelligent Transportation Systems Conf. (ITSC), Auckland, New Zealand, 2019, pp. 1448–1453